Chemical Physics 440 (2014) 99–105

Contents lists available at ScienceDirect

Chemical Physics

journal homepage: www.elsevier.com/locate/chemphys

A theoretical study on the equilibrium structures, vibrational frequencies and photoelectron spectroscopy of thiocarbonyl fluoride by using density functional and coupled-cluster theories

Cyong-Huei Huang, Chiing-Chang Chen, Yu-Kuei Chen, Shih-Chieh Tsai, Jia-Lin Chang *

Department of Science Application and Dissemination, National Taichung University of Education, Taichung 403, Taiwan, ROC

ARTICLE INFO

Article history:
Received 4 February 2014
In final form 18 June 2014
Available online 27 June 2014

Keywords:
Photoelectron spectroscopy
Franck–Condon factor
Density functional theory
Coupled-cluster theory
Thiocarbonyl fluoride

ABSTRACT

The equilibrium geometries, vibrational frequencies and normal modes of F_2CS and F_2CS^+ $\widetilde{X}^2B_2$, $\widetilde{A}^2B_1$, and $\widetilde{B}^2A_1$ states were obtained by utilizing both density functional and coupled-cluster (CC2) theories. Franck–Condon factors were calculated by using the harmonic-oscillator model taking into account the Duschinsky effect, based on which photoelectron spectra were simulated. The adiabatic ionization energies were computed by the CCSD(T) method extrapolated to the complete basis set limit. The computed equilibrium structures and vibrational frequencies are generally in agreement with the experiment, except in few cases. The B3LYP and CC2 approaches perform equally well in the computations of F_2CS. The simulated photoelectron spectra of F_2CS are also in accord with the experiment, indicating that the calculated structures are reliable. The computed adiabatic ionization energies are in agreement with the experiment within 0.01, 0.02, and 0.06 eV for the three ionic states, respectively.

1. Introduction

The vibronic spectroscopy of molecules provides rich information about the equilibrium structures and vibrational energy levels of corresponding electronic states, which can be investigated theoretically by computing molecular properties together with Franck–Condon factors (FCFs) [1–20]. The FCF is the square of the Franck–Condon integral (FCI) which is defined as the integral of the product of vibrational wavefunctions of two electronic states [21–23]. In recent years, we have developed an analytical approach for computing FCIs of harmonic oscillators [24–29]. The Duschinsky effect [30] arising from mixing of vibrational normal coordinates between two electronic states of different equilibrium structures is explicitly treated in our approach. In the latest progress of our methodology, a general formula of FCI of harmonic oscillators with arbitrary dimensions has been derived and applied to study the photoelectron spectrum of ovalene ($C_{32}H_{14}$), a molecule possessing 132 normal modes [29]. Our approach is alternative to other relevant techniques (e.g., [1–20]) and the mature of FCI algorithms has made the theoretical studies of vibronic spectra of molecules convenient and compatible to experiments.

The experimental techniques of molecular photoelectron spectroscopy have been well developed since the 1970s [31,32]. However, theoretical methods capable of computing FCFs of polyatomic molecules were rare when a large number of molecular photoelectron spectra had been recorded. As a consequence, the experimental photoelectron spectra reported in that time were usually assigned according to empirical principles in conjunction with some theoretical computations of orbital energies. It might happen that the assignments were incorrectly made due to the lack of theoretical predictions about spectral patterns. For example, the first peak in the photoelectron spectrum of $H_2O^+(\widetilde{B}^2B_2)$ state was assigned to the adiabatic transition by experimentalists, but Chang's computation indicated that it should correspond to the (0, 2, 0) vibrational state [26]. Similar inconsistency was also found for $D_2O^+(\widetilde{B}^2B_2)$ where the first peak was better interpreted as the transition to the (0, 4, 0) vibrational state [26]. Accordingly, we claim that a reliable assignment of experimental vibronic (including photoelectron) spectra should be in harmony with FCF computations, provided that the model for calculating FCFs is adequate. On the other hand, the observed vibronic spectrum serves as a means to evaluate whether the computed equilibrium structures of excited (or ionic) states are in accord with experimental evidence, since the spectral patterns depend largely on the geometrical differences between the ground and excited (or ionic) states.

In this article, we present a theoretical study on the equilibrium structures, vibrational frequencies and photoelectron spectroscopy of thiocarbonyl fluoride (F_2CS). This compound was first prepared and isolated in 1962 by Downs who was also the first to identify

* Corresponding author. Tel.: +886 4 2218 3564; fax: +886 4 2218 3560.
E-mail address: jlchang@mail.ntcu.edu.tw (J.-L. Chang).

http://dx.doi.org/10.1016/j.chemphys.2014.06.012
0301-0104/

all of its fundamental vibrations by recording the infrared spectra [33,34]. In 1965, Middleton et al. prepared F_2CS by the pyrolysis of its dimer, $(CSF_2)_2$ [35]. Later, Moule and Subramaniam carried out normal coordinate analyses for the five in-plane vibrational modes of F_2CS [36]. Hopper et al. measured the absolute intensities of infrared bands and obtained the normal coordinates of all six vibrational modes of F_2CS [37]. Hass et al. reported the gas phase and matrix infrared spectra as well as liquid phase Raman spectra of F_2CS around 1976 [38,39]. High resolution Fourier transform infrared spectra of F_2CS were reported and analyzed by Bürger and Jerzembeck [40] in 1998 and by Flaoud et al. [41] in 1999. On the other hand, the microwave spectrum of F_2CS was first reported by Careless et al. in 1973 [42]. They also determined the equilibrium structure of F_2CS, in which the bond length R_{CS} = 158.9 pm, R_{CF} = 131.5 pm, and the bending angle A_{FCF} = 107.1° [42]. In 1992, Xu et al. recorded the Raman spectrum of F_2CS with a pulsed molecular-beam microwave Fourier transform spectrometer and reported the structure as R_{CS} = 158.70 pm, R_{CF} = 131.82 pm and A_{FCF} = 106.89° [43].

The electronic absorption spectra of F_2CS were investigated by Moule and co-workers in the 1970s for the singlet–singlet $\pi^* \leftarrow n$, $\pi^* \leftarrow \pi$ and singlet–triplet $\pi^* \leftarrow n$ transitions [44–46]. It was found that the structures in the corresponding excited states are nonplanar and the potential has double wells along the coordinate of the out-of-plane bending mode (ν_4). Recently in 2009, Zeng et al. discovered that matrix isolated F_2CS can photoisomerize to form cis- and trans-FCSF [47]. They also performed theoretical calculations to identify the possible pathways of photoisomerization. Earlier theoretical studies of F_2CS can be found in [48–54].

The photoelectron spectrum of F_2CS was reported by Kroto and Suffolk [55] in 1972 and by Mines et al. [56] in 1973. However, no theoretical studies on the structures of experimental spectrum were available since their publications, which was the motivation of the present study. In the experimental spectrum, some ionic states show clear vibrational structures. It is interesting that both F_2CS^+(X) and F_2CS^+(B) states have a hot band in their spectrum, whereas no hot bands are observed in F_2CS^+(A) [55,56]. An accurate computation of FCFs should be able to account for the vibrational structures observed in different ionic states of F_2CS^+, including the temperature effect which is crucial for hot bands. In addition, the relative intensities of hot bands in comparison to that of the origin band provide clues to determine the vibrational temperature of the experimental sample.

In this work, we computed the equilibrium geometries and vibrational frequencies of F_2CS and three lowest-lying ionic states of F_2CS^+ with density functional theories (DFT) and the second-order approximate coupled-cluster (CC2) theories. The results of time-independent and time-dependent DFT as well as the CC2 computations are compared with each other. The photoelectron spectra of F_2CS were simulated by computing FCFs with the approach developed in this group. We will show that both the simulated photoelectron spectra and the computed adiabatic ionization energies of F_2CS are in agreement with the experiment, indicating that the computed equilibrium geometries are reliable.

2. Computational methods

The equilibrium geometries, harmonic vibrational frequencies and normal modes of F_2CS and the three lowest-lying electronic states of F_2CS^+ were obtained by using the DFT approach with the B3LYP, B3PW91, and M06 functionals in conjunction with various basis sets up to aug-cc-pVTZ. The three ionic states studied are of different symmetry species in the C_{2v} point group, and thus can be optimized by using the time-independent DFT since each is the lowest one in energy among the states with the same symmetry. However, the time-dependent DFT [57,58] of B3LYP and M06 were also applied to calculate the excited states of F_2CS^+ in order to compare the results with those obtained by time-independent DFT. In the time-dependent DFT computations, the geometries were first obtained by using symmetry constraints (C_{2v} point group). Then, the optimization was redone without symmetry constraints (C_1 point group) starting from a structure slightly distorted from the symmetric one. It was found that both the F_2CS^+ $\widetilde{A}$ and $\widetilde{B}$ states converged to the C_{2v} structures as predicted by symmetry constraints. Besides, the CC2 computation employing the-resolution-of-identity approximation [59–61] was performed under the C_1 point group and its results were consistent with those obtained by DFT. In other words, the present study shows that all the ionic states investigated belong to the C_{2v} point group.

With the data of equilibrium geometries, vibrational frequencies, and normal modes as inputs, the FCFs were computed by using the approach developed in this group in which the harmonic-oscillator model including the Duschinsky effect was coded [29]. Then, the photoelectron spectrum was simulated by summing the contributions from possible transitions in which FCFs were taken as the peak heights and the Gaussian function as the line shape. The adiabatic ionization energies (AIEs) were obtained by utilizing the CCSD(T) energies extrapolated to the complete basis set (CBS) limit [62] with aug-cc-pVXZ (X = D, T, Q, 5), in which the equilibrium geometries and zero-point energy (ZPE) corrections were taken from the B3LYP/aug-cc-pVTZ computation. While the DFT and CCSD(T) computations were performed by means of the Gaussian 09 package [63], the CC2 calculations were executed by the Turbomole programs [64].

3. Results and discussion

3.1. Equilibrium structures

Table 1 lists the optimized geometries of the ground state of $F_2CS(\widetilde{X}^1A_1)$ and the ionic states of $F_2CS^+(\widetilde{X}^2B_2$, $\widetilde{A}^2B_1$ and $\widetilde{B}^2A_1)$. As mentioned previously, all of the states studied belong to the C_{2v} point group. For F_2CS, our calculations are generally in agreement

Table 1
Calculated and experimental equilibrium structures of F_2CS and F_2CS^+.

Method[a]	$F_2CS(\widetilde{X}^1A_1)$			$F_2CS^+(\widetilde{X}^2B_2)$		
	R_{CS}	R_{CF}	A_{FCF}	R_{CS}	R_{CF}	A_{FCF}
B3LYP/6-311+G(3df)	159.45	131.40	107.2°	166.54	126.23	115.5°
B3LYP/AVTZ	159.84	131.67	107.2°	167.09	126.48	115.6°
B3PW91/AVTZ	159.60	131.08	107.4°	166.67	126.06	115.8°
M06/AVTZ	159.71	130.00	107.5°	166.61	125.09	115.8°
MP2/6-311+G(3df) [b]	159.0	131.1	107.1°			
CBS-QB3[b]	159.8	131.6	107.4°			
Experiment[c]	158.9	131.5	107.1°			
Experiment[d]	158.70	131.82	106.89°			
Method	$F_2CS^+(\widetilde{A}^2B_1)$			$F_2CS^+(\widetilde{B}^2A_1)$		
	R_{CS}	R_{CF}	A_{FCF}	R_{CS}	R_{CF}	A_{FCF}
B3LYP/6-311+G(3df)	173.56	125.27	114.0°	166.18	126.77	118.4°
B3LYP/AVTZ	174.15	125.53	114.1°	166.69	127.02	118.5°
B3PW91/AVTZ	173.45	125.16	114.2°	166.02	126.54	118.6°
M06/AVTZ	173.38	124.22	114.4°	166.11	125.20	118.8°
TD/B3LYP/AVTZ	173.90	125.59	114.2°	166.37	127.18	117.9°
TD/M06/AVTZ	173.71	124.13	114.6°	168.67	124.82	119.4°
CC2/AVTZ	173.52	125.49	114.2	164.64	127.23	117.9

[a] AVTZ stands for aug-cc-pVTZ, *R* for bondlength (in pm), and *A* for bending angle.
[b] Ref. [47].
[c] Ref. [42].
[d] Ref. [43].

with the experiment within 1 pm for R_{CS}, 0.5 pm for R_{CF}, and 0.2° for A_{FCF}, except for M06/AVTZ in which R_{CF} is 1.5 pm less than the experimental value (Table 1). The MP2 and CBS-QB3 computational results of Zeng et al. [47] are also given in Table 1 for comparison. Table 1 indicates that the variation of results between different approaches is minor and thus the following discussion refers to the B3LYP/AVTZ computation for simplicity.

For the ground state of F_2CS^+, it can be seen from Table 1 that R_{CS} elongates for 7.25 pm, R_{CF} shortens by 5.19 pm, and A_{FCF} opens for 8.4° upon ionization of F_2CS. The geometrical change can be interpreted from the character of orbital originally occupied by the ejected electron. The orbitals obtained in the present study are similar to those reported by Zeng et al. [47]. The highest-occupied molecular orbital (HOMO) of F_2CS is of B_2 symmetry species and is dominated by the nonbonding orbital of the S atom. Its shape is similar to a p orbital of the S atom. However, this orbital has some bonding character between the C and S atoms and some antibonding character between the C and F atoms. As a result, removing a HOMO electron leads to lengthening the CS bond and shortening the CF bond. The reduced electron density in the CS moiety also weakens the repulsion between CS and CF bonds, and therefore A_{FCF} of $F_2CS^+(\widetilde{X}^2B_2)$ is larger than that of F_2CS.

For the first excited state of F_2CS^+, $\widetilde{A}^2B_1$, the bondlength of R_{CS} is 174.11 pm which lengthens to a large extent by about 14.31 pm relative to the neutral molecule (Table 1). On the other hand, R_{CF} shortens by 6.14 pm and A_{FCF} opens for 6.9°. The differences of optimized geometrical parameters between the DFT and CC2 approaches are minor (Table 1). The corresponding orbital is π bonding between the CS bond but antibonding between the C and F atoms. The drastic change of the CS bond stems from removing an electron from the π orbital.

The second ionic excited state, $F_2CS^+(\widetilde{B}^2A_1)$, undergoes similar geometrical change in which the differences are +6.85 pm, −4.65 pm and +11.3° for R_{CS}, R_{CF} and A_{FCF}, respectively. R_{CS} calculated by CC2 is about 2 pm slightly shorter than by B3LYP, and R_{CF} and A_{FCF} are even similar (Table 1). The corresponding orbital is another nonbonding orbital of the S atom which is directed along the CS bond. Meanwhile, it also has some bonding character between the C and S atoms and some antibonding character between the C and F atoms. Accordingly, the ionization process leads to lengthening of R_{CS} and shortening of R_{CF}. The opening of A_{FCF} in this state is larger than in the $\widetilde{X}$ and $\widetilde{A}$ states because this orbital has some bonding character between the two F atoms. Therefore, removing an electron from this orbital results in a longer distance of the F atoms.

Some remarks about the optimization of the $F_2CS^+(\widetilde{B}^2A_1)$ state are given below. Under the C_1 point group, both the time-dependent DFT and the CC2 computations indicate that there

Table 2
Calculated and experimental harmonic vibrational frequencies (cm^{-1}) of F_2CS and F_2CS^+.

State[a]	Mode	ν_1	ν_2	ν_3	ν_4	ν_5	ν_6
	Symmetry species	a_1	a_1	a_1	b_1	b_2	b_2
	Method	Type					
		CS stretch	CF_2 s. stretch	CF_2 scissor	CF_2 wag	CF_2 a. stretch	CF_2 rock
$\widetilde{X}$	B3LYP/6-311+G(3df)	1358	799	528	635	1184	421
	B3LYP/AVTZ	1352	795	525	629	1182	419
	B3PW91/AVTZ	1376	807	530	637	1214	422
	M06/AVTZ	1388	824	540	646	1248	424
	MP2/6-311+G(3df)[b]	1408.3	807.7	535.7	644.6	1213.0	427.0
	CBS-QB3[b]	1356.5	793.7	524.9	628.3	1203.5	418.4
	Experiment[c]	1368	787	526	622	1189	417
	Experiment[d]	1366.7	789.5	526.7	623.2	1190.1	419.5
$\widetilde{X}^+$	B3LYP/6-311+G(3df)	1396	797	490	641	1448	333
	B3LYP/AVTZ	1392	793	488	636	1446	333
	B3PW91/AVTZ	1414	804	492	642	1475	334
	M06/AVTZ	1448	821	501	656	1518	329
	Experiment[e]	1380		450			
	Experiment[f]	1307	758	460			
$\widetilde{A}^+$	B3LYP/6-311+G(3df)	1357	761	487	594	1475	373
	B3LYP/AVTZ	1353	756	482	589	1473	370
	B3PW91/AVTZ	1374	767	491	596	1500	374
	M06/AVTZ	1412	780	498	607	1549	377
	TD/B3LYP/AVTZ	1357	757	483	590	1475	372
	TD/M06/AVTZ	1416	780	496	610	1557	388
	CC2/AVTZ	1371	758	492	601	1487	371
	Experiment[e]	1320–1430	710				
	Experiment[f]	1315	752	482			
$\widetilde{B}^+$	B3LYP/6-311+G(3df)	1180	761	498	642	1376	428
	B3LYP/AVTZ	1174	755	495	637	1373	426
	B3PW91/AVTZ	1209	773	502	649	1411	432
	M06/AVTZ	1263	789	512	674	1487	436
	TD/B3LYP/AVTZ	1142	767	498	642	1339	430
	TD/M06/AVTZ	1255	775	516	665	1532	482
	CC2/AVTZ	1234	779	501	671	1385	434
	Experiment[e]	1160–1280		530			
	Experiment[f]	1159	694	462			

[a] $\widetilde{X}$, $\widetilde{X}^+$, $\widetilde{A}^+$ and $\widetilde{B}^+$ correspond to $F_2CS(\widetilde{X}^1A_1)$, $F_2CS^+(\widetilde{X}^2B_2)$, $F_2CS^+(\widetilde{A}^2B_1)$ and $F_2CS^+(\widetilde{B}^2A_1)$, respectively.
[b] Ref. [47].
[c] Ref. [34].
[d] Ref. [41].
[e] Ref. [55].
[f] Ref. [56].

exists an ionic state between $F_2CS^+(\widetilde{A}^2B_1)$ and $F_2CS^+(\widetilde{B}^2A_1)$. However, the formation of this ionic state involves an extra excitation of an electron from the 19a orbital to 21a, in addition to the ionization of an electron from the 20a (HOMO) orbital. Such a process cannot be observed in conventional one-photon photoelectron spectroscopy [31,32] and therefore we do not probe it further in the present study. In addition, the successful optimization of $F_2CS^+(\widetilde{B}^2A_1)$ (the third root of excited state) was achieved by including four and nine excited states in the CC2 and DFT computations, respectively.

3.2. Vibrational frequencies

Table 2 lists the harmonic vibrational frequencies of F_2CS and F_2CS^+. For F_2CS, the computed harmonic vibrational frequencies are generally in agreement with the experiments. At the B3LYP/AVTZ level, ν_1 is 15 cm^{-1} smaller than the experimental value while the other modes agree with the experiments within 8 cm^{-1}. This approach also performs equally well with the CBS-QB3 method [47] (Table 2). At the M06/AVTZ level, however, the deviation is noticeable and the greatest one refers to ν_5 (+58 cm^{-1}).

For the ground state of F_2CS^+, there are two sets of experimental values available (Table 2). Kroto and Suffolk [55] determined the vibrational frequency of ν_1 as 1380 cm^{-1} while Mines et al. [56] 1307 cm^{-1}. Our computation is in line with the measurement of Ktoto and Suffolk (Table 2). The frequencies of ν_2 and ν_3 obtained at the B3LYP/AVTZ level are in accord with the experiments within 35 cm^{-1}. The deviations of B3PW91 and M06 computations with respect to experimental values are larger than those of the other approaches used (Table 2).

The vibrational frequencies of $F_2CS^+(\widetilde{A}^2B_1)$ calculated at the B3LYP/AVTZ level (Table 2) are in excellent agreement with the experiment: ν_1, ν_2 and ν_3 are larger than the experimental values by 38, 4 and 0 cm^{-1}, respectively. Both time-dependent and time-independent B3LYP/AVTZ computations give similar results, so do the M06/AVTZ and the CC2 calculations (Table 2). Nevertheless, ν_1 obtained by the M06 functional is subject to a larger deviation, about +100 cm^{-1} (Table 2).

For $F_2CS^+(\widetilde{B}^2A_1)$, ν_1 (1174 cm^{-1}) and ν_2 (755 cm^{-1}) computed by B3LYP/AVTZ are respectively 15 and 61 cm^{-1} larger than those determined by Mines et al. [56] (Table 2), while ν_3 (495 cm^{-1}) is close to the average (496 cm^{-1}) of the two experimental values (530 and 462 cm^{-1}). The vibrational frequencies obtained by the time-dependent and time-independent B3LYP/AVTZ approaches are slightly different, but their absolute deviations relative to the experiment are similar. The vibrational frequencies obtained by the CC2/AVTZ approach are in harmony with those by B3LYP/AVTZ. Nevertheless, the deviations between theory and experiment are larger when using the M06 approaches (Table 2).

We now summarize the performance of different methods on predicting the vibrational frequencies of F_2CS and F_2CS^+. Within the basis sets utilized, while the results of B3LYP, time-independent B3PW91 and CC2 computations are all in accord with the experiments, the M06 approach is less satisfactory.

3.3. Photoelectron spectrum

The simulated photoelectron spectra of F_2CS with different approaches of this work are similar and we show only those computed at the B3LYP/AVTZ level for simplicity. Fig. 1 depicts the simulated photoelectron spectra of F_2CS for transitions from the vibrational ground state and two vibrational excited states to form the electronic ground state of $F_2CS^+(\widetilde{X}^2B_2)$. The abscissa in each figure is the excitation energy relative to the adiabatic transition (0_0^0). The vibrational excited states of F_2CS were included in the simulation because the hot band of 3_1^0 was observed by Ktoto and

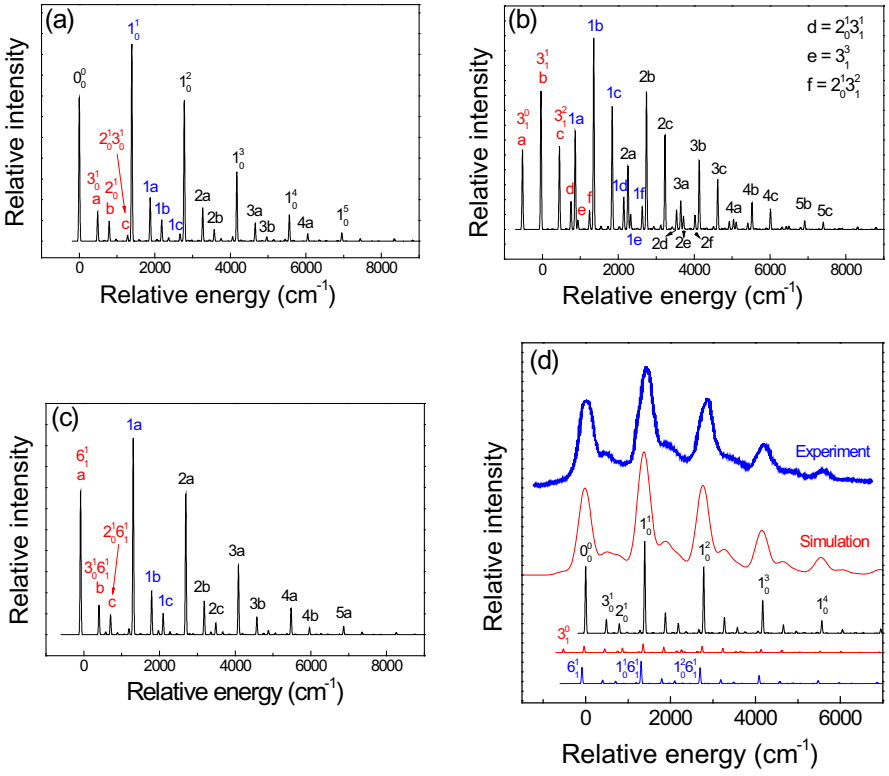

Fig. 1. The simulated photoelectron spectrum of F_2CS ionized from the (a) vibrationless, (b) $\nu_3 = 1$, and (c) $\nu_6 = 1$ state to form $F_2CS^+(\widetilde{X}^2B_2)$ (FWHM = 30 cm^{-1}). The simulated overall spectrum at 425 K is shown in (d) with FWHM = 350 cm^{-1}, which is in agreement with the experiment (Reproduced from Chem. Phys. Lett. 17 (1972) 213, with permission from Elsevier).

Suffolk [55] and also by Mines et al. [56] We included another hot band, 6_1^0, in the simulation because the vibrational frequency of ν_6 (419.5 cm^{-1}) is lower than ν_3 (526.7 cm^{-1}), and hence ν_6 should have a greater population than ν_3 and the other modes. We have also simulated some hot bands with higher energies, but their contributions to the spectrum are minor and therefore not shown here.

Fig. 1a shows that the progressions of ν_1 and the combination bands of ν_1, ν_2 and ν_3 constitute the main feature of the spectrum for ionizations from the vibrational ground state of F_2CS. The three totally symmetric modes are active in the spectrum owing to their appreciable geometrical changes upon ionization. In this article, some repeating structures in the spectrum are labeled with alphabets for simplicity. For example, the transitions 3_0^1, 2_0^1 and $2_0^1 3_0^1$ are labeled with a, b and c, and their combinations with the nth quantum of ν_1 are denoted as na, nb and nc, respectively. In Fig. 1a, 1a stands for $1_0^1 3_0^1$, 2b for $1_0^2 2_0^1$, and 1c for $1_0^1 2_0^1 3_0^1$, etc. The spectral pattern arising from the 3_1^0 hot bands (Fig. 1b) is distinct from that of Fig. 1a, but that arising from 6_1^0 (Fig. 1c) is similar to the cold bands (Fig. 1a). Fig. 1d shows the comparison of the simulated and experimental photoelectron spectra corresponding to $F_2CS^+(\tilde{X}^2B_2)$. The spectrum contributed from different initial vibrational states was weighted by its population according to the Boltzmann distribution law. This approach is complementary to the techniques by which the electronic spectrum can be simulated without detailed computations of FCF, e.g., the generating function method [65–71]. In this work, we adjusted the vibrational temperature until the simulated spectrum fitted the experiment for all the three ionic states studied. It was found that the vibrational temperature was about 425 K in the experiment of Kroto and Suffolk [55]. It can be seen that the spectrum simulated with the full-width at half maximum (FWHM) of 350 cm^{-1} is in good agreement with the experiment (Fig. 1d). Moreover, the theoretical study provides detailed structures of the spectrum which are beyond one can identify from the experimental spectrum. It was found that transitions from the vibrationless state dominate the spectrum, those from $\nu_3 = 1$ have small intensities, and the transitions 6_1^1, $1_0^1 6_1^1$ and $1_0^2 6_1^1$ are non-negligible but difficult to be detected because of their overlapping with the stronger 0_0^0, 1_0^1 and 1_0^2 bands (Fig. 1d). The role of hot bands arising from $\nu_6 = 1$ were not noticed by the previous experimental studies [55,56].

Figs. 2a–c show the simulated photoelectron spectra corresponding to $F_2CS^+(\tilde{A}^2B_1)$ for ionizations arising from the vibrationless, $\nu_3 = 1$ and $\nu_6 = 1$ states, respectively. As mentioned above, this ionic state is formed by removing a CS π electron accompanying drastic geometrical changes, which are responsible for the complex structures in the photoelectron spectra. The spectral patterns of Fig. 2a and c resemble each other, whereas Fig. 2b is more complicated and the repeating structure involves eight transitions (a–h). Fig. 2d shows individual contributions from different initial vibrational states together with the whole simulated spectrum. The signals of hot bands are likely to be buried by the cold bands and should be indiscernible in the spectrum. The small FCF value of 3_1^0 (Fig. 2b), which is the key transition for the identification of hot bands, is due to the larger geometrical change of this state compared to the ground state of F_2CS. As shown in Table 1, all

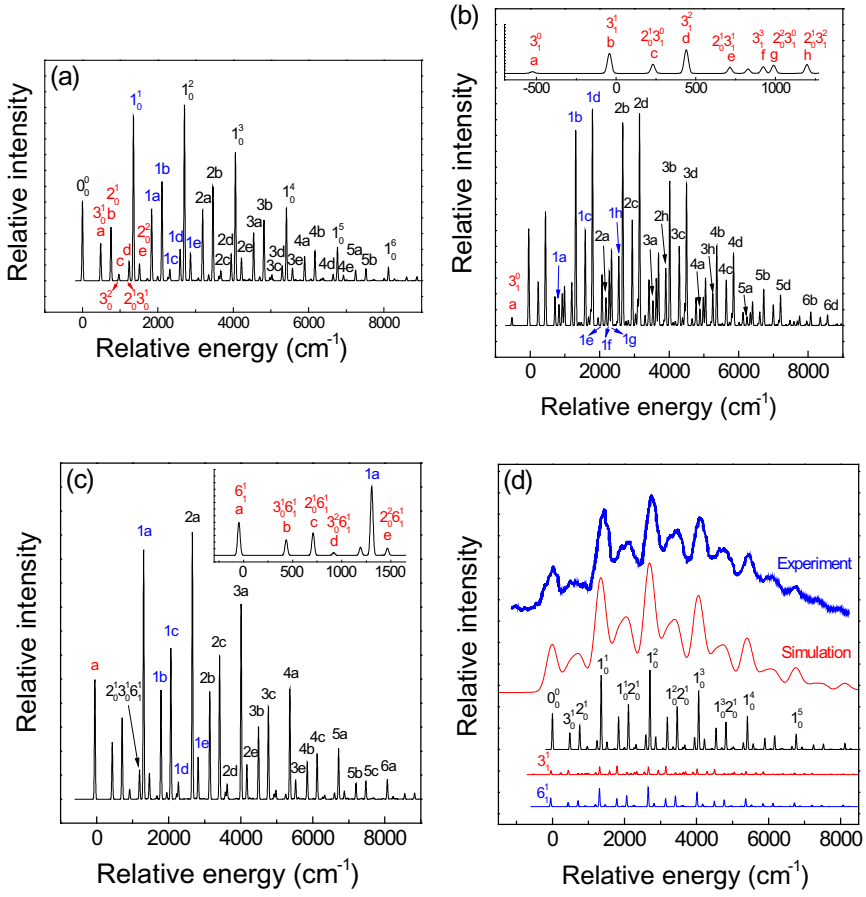

Fig. 2. The simulated photoelectron spectrum of F_2CS ionized from the (a) vibrationless, (b) $\nu_3 = 1$, and (c) $\nu_6 = 1$ state to form $F_2CS^+(\tilde{A}^2B_1)$ (FWHM = 30 cm^{-1}). The simulated overall spectrum at 425 K is shown in (d) with FWHM = 350 cm^{-1}, which is in agreement with the experiment (Reproduced from Chem. Phys. Lett. 17 (1972) 213, with permission from Elsevier).

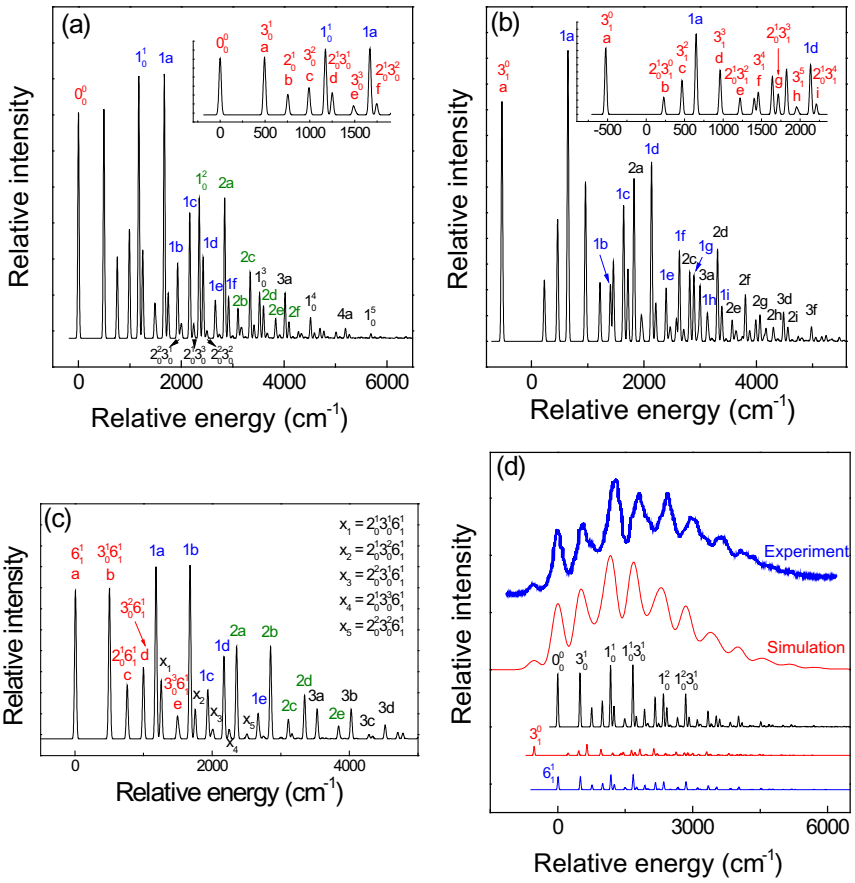

Fig. 3. The simulated photoelectron spectrum of F_2CS ionized from the (a) vibrationless, (b) $\nu_3 = 1$, and (c) $\nu_6 = 1$ state to form $F_2CS^+(\tilde{B}^2A_1)$ (FWHM = 30 cm^{-1}). The simulated overall spectrum at 425 K is shown in (d) with FWHM = 300 cm^{-1}, which is in agreement with the experiment (Reproduced from Chem. Phys. Lett. 17 (1972) 213, with permission from Elsevier).

Table 3
Calculated CCSD(T) energies (in hartree) and adiabatic ionization energies (AIE, in eV) of F_2CS.

n	Basis set	$F_2CS(\tilde{X}^1A_1)$	$F_2CS^+(\tilde{X}^2B_2)$	$F_2CS^+(\tilde{A}^2B_1)$	$F_2CS^+(\tilde{B}^2A_1)$
2	AVDZ	−634.98814	−634.61205	−634.57823	−634.44745
3	AVTZ	−635.24164	−634.86168	−634.82912	−634.69693
4	AVQZ	−635.32039	−634.93785	−634.90513	−634.77327
5	AV5Z	−635.34716	−634.96363	−634.93076	−634.79892
∞	CBS limit[a]	−635.36372(75)	−634.97960(74)	−634.94668(78)	−634.81497(85)
	This work[b]		10.46	11.36	14.93
	Theory[c]		10.42		
	Experiment[d]		10.45	11.34	14.87
	Experiment[e]		10.52	11.39	14.91

[a] Values in parentheses are errors in the last digit.
[b] Theoretical AIE values computed by the CCSD(T) CBS limit approach with zero-point energy correction at the B3LYP/aug-cc-pVTZ level.
[c] The theoretical AIE value computed by the G4 approach, taken from Ref. [72].
[d] Experimental AIE values taken from Ref [55].
[e] Experimental AIE values taken from Ref. [56].

R_{CS}, R_{CF} and A_{FCF} of $F_2CS^+(\tilde{A}^2B_1)$ undergo substantial variations upon ionization, whereas the change of R_{CS} in the other two ionic states is smaller. As a consequence, the displacements of the corresponding normal modes (ν_1–ν_3) for $F_2CS^+(\tilde{A}^2B_1)$ are greater and thus the spectrum is dominated by the stronger combination bands accompanying the weaker 3_1^0 transition (Fig. 2b). This interpretation is consistent with the experimental observations (Fig. 2d).

The simulated photoelectron spectra corresponding to $F_2CS^+(\tilde{B}^2A_1)$ are shown in Fig. 3. Due to the larger change of A_{FCF} (+11.3°), the progression of ν_3 (CF_2 scissor) is longer than that in the other two states. For instance, 3_0^3 and $3_0^3 6_1^1$ are present in the spectrum of Fig. 3a and c, respectively, and 3_1^5 in Fig. 3b. Similarly, the progression of ν_1 (CS stretch) is extended to 1_0^5 (Fig. 3b) due to the substantial change in R_{CS} (+6.85 pm). Five transitions (x_1–x_5 in Fig. 3c) involving the excitation of three normal modes are observed in the simulated spectrum originating from the $\nu_6 = 1$ state. However, these transitions do not appear in the repeating structure, reflecting the fact that the probability of simultaneous excitation of four modes is greatly reduced in comparison to that of three-mode excitations. The overall simulated spectrum is

shown in Fig. 3d. Importantly, the present study infers that the hot band of 3_1^0 is well separated from 0_0^0 and its intensity is strong enough to be detected, in agreement with the experiment (Fig. 3d) [55,56].

3.4. Adiabatic ionization energy

The AIEs of F_2CS computed by the CBS limit method are listed in Table 3. The AIE of F_2CS calculated by Rayne and Forest with the G4 approach is 10.42 eV [72], 0.04 eV smaller than this work (Table 3). In comparison with experimental values, the theoretical ones of 10.46, 11.36 and 14.93 eV of this work are in agreement with those determined by Kroto and Suffolk [55] within 0.01, 0.02 and 0.06 eV, and are also in accord with those reported by Mines et al. [56] within −0.06, −0.03 and 0.02 eV, respectively (Table 3). Accordingly, the present theoretical study is consistent with the experiments in both the spectral patterns and AIEs, meaning that the equilibrium structures, vibrational frequencies, and spectral assignments of this work are reliable.

4. Conclusions

By computing Franck–Condon factors with the approach developed in this group, the photoelectron spectroscopy of F_2CS has been investigated in detail. The equilibrium geometries, harmonic vibrational frequencies, and normal modes of F_2CS and F_2CS^+ $\widetilde{X}^2B_2$, $\widetilde{A}^2B_1$ and $\widetilde{B}^2A_1$ states were computed by using density functional theories. The time-dependent density functional theory and the CC2 approach were also adopted to calculate the excited states of F_2CS^+. The adiabatic ionization energies were obtained by extrapolating the computed CCSD(T) energies to the complete basis set limit. In general, the computed equilibrium geometries and vibrational frequencies are in agreement with the experiments. However, the vibrational frequencies computed by the M06 functional are deviated from the experimental values to a larger extent. The simulated photoelectron spectra are in harmony with the experiment. The time-independent and time-dependent B3LYP approaches perform equally well in studying F_2CS, so does the CC2. The match between theory and experiment in both the adiabatic ionization energy and the spectral pattern infers that the quantum chemistry computations of the present study are reliable.

Conflict of interest

There is no conflict of interest.

Acknowledgments

This work is supported by the National Science Council of the Republic of China (Grant No. NSC 100-2113-M-142-001-MY3). We are grateful to the National Center for High-performance Computing for computer time and facilities.

References

[1] T.E. Sharp, H.M. Rosenstock, J. Chem. Phys. 41 (1964) 3453.
[2] E.V. Doktorov, I.A. Malkin, V.I. Man'ko, J. Mol. Spectrosc. 56 (1975) 1.
[3] L.S. Cederbaum, W. Domcke, J. Chem. Phys. 64 (1970) 603.
[4] H. Kupka, P.H. Cribb, J. Chem. Phys. 85 (1986) 1303.
[5] A.M. Mebel, Y.-T. Chen, S.H. Lin, Chem. Phys. Lett. 258 (1996) 53.
[6] A.M. Mebel, M. Hayashi, K.K. Liang, S.H. Lin, J. Phys. Chem. A 103 (1999) 10674.
[7] P.-Å. Malmqvist, N. Forsberg, Chem. Phys. 228 (1998) 227.
[8] A. Toniolo, M. Persico, J. Comput. Chem. 22 (2001) 968.
[9] D.K.W. Mok, E.P.F. Lee, F.-T. Chau, D.C. Wang, J.M. Dyke, J. Chem. Phys. 113 (2000) 5791.
[10] H. Kikuchi, M. Kubo, N. Watanabe, H. Suzuki, J. Chem. Phys. 119 (2003) 729.
[11] M. Dierksen, S. Grimme, J. Chem. Phys. 122 (2005) 244101.
[12] J.M. Luis, B. Kirtman, O. Christiansen, J. Chem. Phys. 125 (2006) 154114.
[13] V. Rodriguez-Garcia, K. Yagi, K. Hirao, S. Iwata, S. Hirata, J. Chem. Phys. 125 (2006) 014109.
[14] F. Santoro, R. Improta, A. Lami, J. Bloino, V. Barone, J. Chem. Phys. 128 (2008) 224311.
[15] J. Bloino, M. Viczysko, O. Crescenzi, V. Barone, J. Chem. Phys. 128 (2008) 244105.
[16] V. Barone, J. Bloino, M. Biczysko, F. Santoro, J. Chem. Theory Comput. 5 (2009) 540.
[17] R. Grimminger, D.J. Clouthier, R. Tarroni, Z. Wang, T.J. Sears, J. Chem. Phys. 139 (2013) 174306.
[18] J. Harvey, P. Hemberger, A. Bodi, R.P. Tuckett, J. Chem. Phys. 138 (2013) 124301.
[19] D.K.W. Mok, E.P.F. Lee, F.-T. Chau, J.M. Dyke, J. Chem. Phys. 139 (2013) 014301.
[20] J.P. Götze, B. Karasulu, W. Thiel, J. Chem. Phys. 139 (2013) 234108.
[21] J. Franck, Trans. Faraday Soc. 21 (1925) 536.
[22] E. Condon, Phys. Rev. 28 (1926) 1182.
[23] E.U. Condon, Phys. Rev. 32 (1928) 858.
[24] J.-L. Chang, J. Mol. Spectrosc. 232 (2005) 102.
[25] J.-L. Chang, C.-W. Tsao, Chem. Phys. Lett. 428 (2006) 23.
[26] J.-L. Chang, J. Chem. Phys. 128 (2008) 174111.
[27] C.-L. Lee, S.-H. Yang, S.-Y. Kuo, J.-L. Chang, J. Mol. Spectrosc. 256 (2009) 279.
[28] J.-L. Chang, S.-T. Huang, C.-C. Chen, T.-T. Yang, C.-C. Hsiao, H.-Y. Lu, C.-L. Lee, Chem. Phys. Lett. 486 (2010) 12.
[29] J.-L. Chang, C.-H. Huang, S.-C. Chen, T.-H. Yin, Y.-T. Chen, J. Comput. Chem. 34 (2013) 757.
[30] F. Duschinsky, Acta Physicochim. URSS 7 (1937) 551.
[31] D.W. Turner, C. Baker, A.D. Baker, C.R. Brundle, Molecular Photoelectron Spectroscopy, John Wiley & Sons, London, 1970.
[32] S. Hüfner, Photoelectron Spectroscopy: Principles and Applications, Springer-Verlag, Berlin, 2003.
[33] A.J. Downs, J. Chem. Soc. (1962) 4361.
[34] A.J. Downs, Spectrochim. Acta 19 (1963) 1165.
[35] W.J. Middleton, E.G. Howard, W.H. Sharkey, J. Org. Chem. 30 (1965) 1375.
[36] D.C. Moule, C.R. Subramaniam, Can. J. Chem. 47 (1969) 1011.
[37] M.J. Hopper, J.W. Russell, J. Overend, Spectrochim. Acta 28A (1972) 1215.
[38] A. Haas, B. Koch, N. Welcman, H. Willner, Spectrochim. Acta 32A (1976) 497.
[39] A. Haas, H. Willner, H. Burger, G. Pawelke, Spectrochim. Acta 33A (1977) 937.
[40] H. Bürger, W. Jerzembeck, J. Mol. Spectrosc. 188 (1998) 209.
[41] J.-M. Flaud, W. Jerzembeck, H. Bürger, J. Mol. Spectrosc. 197 (1999) 297.
[42] A.J. Careless, H.W. Kroto, B.M. Landsberg, Chem. Phys. 1 (1973) 371.
[43] Y. Xu, M.C.L. Gerry, D.L. Joo, D.J. Clouthier, J. Chem. Phys. 97 (1992) 3931.
[44] D.C. Moule, A.K. Mehra, J. Mol. Spectrosc. 35 (1970) 137.
[45] D.C. Moule, Can. J. Chem. 48 (1970) 2623.
[46] C.R. Lessard, D.C. Moule, Spectrochim. Acta 29A (1973) 1085.
[47] X. Zeng, H. Beckers, H. Willner, Chem. Commun. (2009) 5162.
[48] R.E. Bruns, J. Chem. Phys. 58 (1973) 1855.
[49] A.B.M.S. Bassi, R.E. Bruns, J. Chem. Phys. 62 (1975) 3235.
[50] R.E. Bruns, J. Chem. Phys. 64 (1976) 3084.
[51] A. Kapur, R.P. Steer, P.G. Mezey, J. Chem. Phys. 69 (1978) 968.
[52] B. Simard, A.E. Bruno, P.G. Mezey, R.P. Steer, Chem. Phys. 103 (1986) 75.
[53] B. Nikolova, B. Galabov, C. Lozanova, J. Chem. Phys. 78 (1983) 4828.
[54] S.H.D.M. Faria, J.V. da Silva Jr., R.L.A. Haiduke, L.N. Vidal, P.A.M. Vazquez, R.E. Bruns, J. Phys. Chem. A 111 (2007) 7870.
[55] H.W. Kroto, R.J. Suffolk, Chem. Phys. Lett. 17 (1972) 213.
[56] G.W. Mines, R.K. Thomas, S.H. Thompson, Proc. R. Soc. A 333 (1973) 171.
[57] F. Furche, R. Ahlrichs, J. Chem. Phys. 117 (2002) 7433.
[58] G. Scalmani, M.J. Frisch, B. Mennucci, J. Tomasi, R. Cammi, V. Barone, J. Chem. Phys. 124 (2006) 094107.
[59] O. Christiansen, H. Koch, P. Jørgensen, Chem. Phys. Lett. 243 (1995) 409.
[60] C. Hättig, F. Weigend, J. Chem. Phys. 113 (2000) 5154.
[61] A. Kohn, C. Hättig, J. Chem. Phys. 119 (2003) 5021.
[62] K.A. Peterson, D.E. Woon, T.H. Dunning Jr., J. Chem. Phys. 100 (1994) 7410.
[63] M.J. Frisch, G.W. Trucks, H.B. Schlegel, G.E. Scuseria, M.A. Robb, J.R. Cheeseman, G. Scalmani, V. Barone, B. Mennucci, G.A. Petersson, H. Nakatsuji, M. Caricato, X. Li, H.P. Hratchian, A.F. Izmaylov, J. Bloino, G. Zheng, J.L. Sonnenberg, M. Hada, M. Ehara, K. Toyota, R. Fukuda, J. Hasegawa, M. Ishida, T. Nakajima, Y. Honda, O. Kitao, H. Nakai, T. Vreven, J.A. Montgomery, J.E. Peralta Jr., F. Ogliaro, M. Bearpark, J.J. Heyd, E. Brothers, K.N. Kudin, V.N. Staroverov, R. Kobayashi, J. Normand, K. Raghavachari, A. Rendell, J.C. Burant, S.S. Iyengar, J. Tomasi, M. Cossi, N. Rega, J.M. Millam, M. Klene, J.E. Knox, J.B. Cross, V. Bakken, C. Adamo, J. Jaramillo, R. Gomperts, R.E. Stratmann, O. Yazyev, A.J. Austin, R. Cammi, C. Pomelli, J.W. Ochterski, R.L. Martin, K. Morokuma, V.G. Zakrzewski, G.A. Voth, P. Salvador, J.J. Dannenberg, S. Dapprich, A.D. Daniels, O. Farkas, J.B. Foresman, J.V. Ortiz, J. Cioslowski, D.J. Fox, Gaussian 09 (Revision A.02), Gaussian Inc., Wallingford, CT, 2009.
[64] TURBOMOLE V6.5 2013, A development of University of Karlsruhe and Forschungszentrum Karlsruhe GmbH, 1989–2007, TURBOMOLE GmbH, since 2007, available from <http://www.turbomole.com>.
[65] M. Lax, J. Chem. Phys. 20 (1952) 1752.
[66] R. Kubo, Y. Toyozawa, Prog. Theor. Phys. 13 (1955) 160.
[67] S. Mukamel, S. Abe, Y.J. Yan, R. Islampour, J. Phys. Chem. 89 (1985) 201.
[68] R. Borrelli, A. Peluso, Phys. Chem. Chem. Phys. 13 (2011) 4420.
[69] J. Huh, R. Berger, Faraday Discuss. 150 (2011) 363.
[70] R. Borrelli, A. Capobianco, A. Peluso, J. Phys. Chem. A 116 (2012) 9934.
[71] R. Borrelli, A. Capobianco, A. Peluso, Can. J. Chem. 91 (2013) 495.
[72] S. Rayne, K. Forest, Comput. Theor. Chem. 974 (2011) 163.